PHYSICAL REVIEW B **80**, 201406(R) (2009)

Stability and work function of TiC_xN_{1-x} alloy surfaces: Density functional theory calculations

H. Zhu, M. Aindow, and R. Ramprasad*

Department of Chemical, Materials and Biomolecular Engineering, Institute of Materials Science, University of Connecticut, 97 North Eagleville Road, Storrs, Connecticut 06269, USA

(Received 10 October 2009; published 20 November 2009)

Critical factors that control the vacuum work function of the TiC_xN_{1-x} ternary system surfaces were determined using detailed density functional theory calculations. Surface chemistry (i.e., orientation, stoichiometry, and defect density) was found to play the most important role in determining the work function value, far surpassing the impact of alloy composition (i.e., x value) on the work function. In general, Ti-deficient surfaces display larger work functions. Work function tuning may thus be effectively accomplished by controlling the surface chemistry rather than the composition.

DOI: 10.1103/PhysRevB.80.201406 PACS number(s): 73.30.+y, 68.35.bd, 71.15.Mb

Our ability to modulate the work function of metals, e.g., through control of composition and/or surface chemistry, is an enabling factor that guides the choice of electrodes in (opto)electronic devices. For instance, present-day transistors (based on SiO_2 insulators) utilize polycrystalline Si electrodes whose work function can be tuned through doping. Next-generation transistors will involve higher dielectric constant insulators and, as a consequence, will require the design and usage of metal gate electrodes with controllable work function values.[1]

TiC_xN_{1-x} is a promising gate electrode, as it can be deposited and processed using methods already well developed in the semiconductor industry. Moreover, its vacuum work function may be tuned by composition modulation.[2] While specific surfaces of the TiC and TiN binaries have been well studied in the past,[3–5] a comprehensive understanding of the critical factors that control the vacuum work function of the TiC_xN_{1-x} ternary alloy system, including composition, surface orientation, and surface chemistry, is currently unavailable. Here, using *ab initio* density functional theory (DFT) based simulations, we have arrived at such an understanding. The strategy and sequence of steps adopted are not specific to the TiC_xN_{1-x} system and essential for a similar study of any multicomponent system.

The TiC_xN_{1-x} alloy was modeled as an ordered phase, and several compositions (i.e., x values) were considered. Of the (001), (110), and (111) types of surfaces with various possible terminations studied, the most stable surfaces were determined to be the ones with the (001) orientation. Although the work function of the most stable surfaces does vary with alloy composition, at any given composition, the work function depends far more significantly on the surface terminations and surface defect chemistry. Work function increases could, in general, be correlated with decreasing surface Ti content (more than bulk alloy composition changes).

Our DFT calculations were performed using the Vienna *ab initio* simulation package (VASP)[6] with the PW91 generalized gradient approximation (GGA),[7] projector-augmented wave pseudopotentials, and a cutoff energy of 350 eV for the plane wave expansion of the wave functions. The choice of the PW91 GGA functional was motivated by its accurate predictions of the geometry, relative surface stability, and electronic structure of transition metal nitrides.[8] Considering TiC and TiN are both stable in the NaCl structure in a wide composition range,[9] we have assumed that TiC_xN_{1-x} also has the same crystal structure and restrict our study to homogeneous NaCl-type TiC_xN_{1-x}. The rhombohedral primitive unit cell of TiN [shown in Fig. 1(a)] contains one Ti and one N atoms. To obtain homogeneous TiC_xN_{1-x} (x=0, 0.25, 0.5, 0.75, and 1), a supercell of TiN with $2\times2\times2$ primitive cells was created, followed by the substitution of an appropriate number of N atoms with C in a systematic way. Figure 1(b) shows the $2\times2\times2$ supercell of pure TiN (containing eight N atoms) and Figs. 1(c) and 1(d) illustrate TiC_xN_{1-x} alloys for x=0.25 (containing six N and two C atoms) and for x=0.5 (containing four N and four C atoms), respectively. The x=0.75 and x=1.0 cases can be obtained by interchanging the identities of the N and C atoms of Figs. 1(c) and 1(b), respectively. These bulk calculations required a $5\times5\times5$ k-point mesh for well converged results. Our surface calculations for the five alloy compositions were performed using slab supercells containing 13 layers. The (001), (110), and (111) surfaces involved 2×2, $2\sqrt{2}\times2$, and 2×2 unit cells along the surface planes and required $5\times5\times1$, $4\times5\times1$, and $5\times5\times1$ k-point meshes, respectively. All slab supercells were subjected to geometry optimization until each component of the force on every atom was smaller than 0.02 eV/Å. These optimizations reproduced the surface relaxations seen earlier in TiN and TiC surfaces.[10]

We begin by presenting bulk TiC_xN_{1-x} results. As Fig. 2 shows, the computed lattice constants of the TiC and TiN end members, as well as the roughly linear variation of the lattice constant across the composition range, are in good agree-

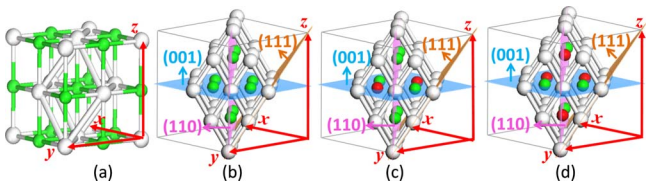

FIG. 1. (Color online) (a) The conventional cubic cell and primitive rhombohedral cell (the latter shown in white) of bulk TiN; (b) the $2\times2\times2$ TiN supercell; and (c) and (d) the supercells of TiC_xN_{1-x} for x=0.25 and x=0.5, respectively. Ti, C, and N atoms are represented by white, red (dark gray), and green (gray) spheres, respectively. The (001), (110), and (111) planes are indicated in the figure.

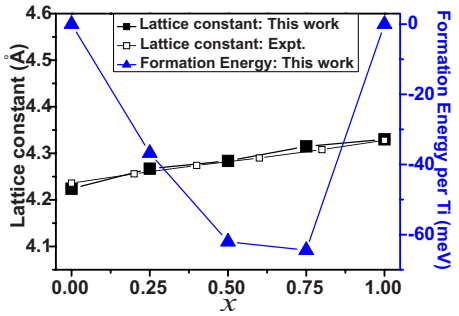

FIG. 2. (Color online) Lattice constants and formation energies per Ti of bulk TiC_xN_{1-x} as a function of x.

ment with available experimental data.[11] Figure 2 also shows the formation energy, E_{form}, of bulk TiC_xN_{1-x} alloys, defined as

$$E_{form} = E_{TiC_xN_{1-x},bulk} - xE_{TiC,bulk} - (1-x)E_{TiN,bulk}, \quad (1)$$

where $E_{TiC_xN_{1-x},bulk}$, $E_{TiC,bulk}$, and $E_{TiN,bulk}$ are the calculated DFT energies per Ti atom of the bulk TiC_xN_{1-x} alloy, pure TiC, and pure TiN, respectively. As the figure shows, the TiC_xN_{1-x} ternary in the NaCl crystal structure is stable to the decomposition to the TiC and TiN binaries, consistent with prior experimental and DFT works.[12,13]

For each of the compositions discussed above, we considered the (001), (110), and (111) surfaces, the normally observed ones for TiC_xN_{1-x}.[14] Depending on the bulk composition and orientation, the stacking sequence of planes and the composition within a plane can vary. Figure 1 shows the three classes of planes considered here, and Table I lists all possible stacking sequences for a given bulk composition and orientation. To study the properties of these possible surfaces, symmetric slabs with identical top and bottom surfaces were created. We note that not all surfaces are "stoichiometric," i.e., not all layers have the same composition as the bulk. For instance, only the (001) and (110) surfaces of TiN, TiC, and $TiC_{0.5}N_{0.5}$ are stoichiometric and hence nonpolar. All other surfaces are polar and hence require the specification of their surface energies in terms of the chemical potentials of the elemental components,[15] as will be described below.

TABLE I. The stacking sequences of TiC_xN_{1-x} along the ⟨001⟩, ⟨110⟩, and ⟨111⟩ directions.

	Bulk composition				
Direction	$x=0$	$x=0.25$	$x=0.5$	$x=0.75$	$x=1$
⟨001⟩ and ⟨110⟩	⋮	⋮	⋮	⋮	⋮
	TiN	$TiC_{0.5}N_{0.5}$	$TiC_{0.5}N_{0.5}$	$TiC_{0.5}N_{0.5}$	TiC
	TiN	TiN	$TiC_{0.5}N_{0.5}$	TiC	TiC
	TiN	$TiC_{0.5}N_{0.5}$	$TiC_{0.5}N_{0.5}$	$TiC_{0.5}N_{0.5}$	TiC
	TiN	TiN	$TiC_{0.5}N_{0.5}$	TiC	TiC
	⋮	⋮	⋮	⋮	⋮
⟨111⟩	⋮	⋮	⋮	⋮	⋮
	Ti	Ti	Ti	Ti	Ti
	N	CN_3	CN	C_3N	C
	Ti	Ti	Ti	Ti	Ti
	N	CN_3	CN	C_3N	C
	⋮	⋮	⋮	⋮	⋮

The surface energy, σ_{surf}, is defined as

$$\sigma_{surf} = (E_{slab} - E_{bulk})/2A, \quad (2)$$

where E_{slab} and E_{bulk} are the energies of the slab and of the bulk material, respectively, containing the same number and type of atoms as the slab. A is the surface area and the factor 2 accounts for the fact that we have two identical surfaces in the supercell. E_{bulk} could be expressed as

$$E_{bulk} = n_{Ti}\mu_{Ti} + n_C\mu_C + n_N\mu_N, \quad (3)$$

where μ_{Ti}, μ_C, and μ_N are the chemical potentials of Ti, C, and N atoms in bulk TiC_xN_{1-x}, respectively, and n_{Ti}, n_C, and n_N are the number of Ti, C, and N atoms in the slab.

Since

$$E_{TiC_xN_{1-x},bulk} = \mu_{Ti} + x\mu_C + (1-x)\mu_N, \quad (4)$$

the surface energy could be specified based on DFT energies and μ_C and μ_N as follows:

$$\sigma_{surf} = \{E_{slab} - n_{Ti}E_{TiC_xN_{1-x},bulk} - (n_C - xn_{Ti})\mu_C - [n_N - (1-x)n_{Ti}]\mu_N\}/2A. \quad (5)$$

We note that for a stoichiometric or nonpolar surface [in which case $n_{Ti}:n_C:n_N = 1:x:(1-x)$] the surface energy is uniquely specified as $\sigma_{surf} = (E_{slab} - n_{Ti}E_{TiC_xN_{1-x},bulk})/2A$, but for polar surfaces, the surface energy is a function of μ_C and μ_N. By treating μ_C and μ_N as free parameters, one could determine the surface energy of the (001), (110), and (111) surfaces with various terminations and bulk compositions. Furthermore, the surface with the lowest surface energy for a given combination of μ_C and μ_N can be determined. This has been done here for all five TiC_xN_{1-x} crystals considered, as displayed in Fig. 3.

We could further specify which surface is the most expected one for a given composition by noting that the possible values μ_C and μ_N can take for a stable ternary alloy are limited by certain constraints.[15] To avoid elemental segregation from the TiC_xN_{1-x} ternary, μ_{Ti}, μ_C, and μ_N should satisfy the following inequalities:

$$\mu_{Ti} \le \mu_{Ti,bulk},$$

$$\mu_C \le \mu_{C,bulk},$$

$$\mu_N \le \mu_{N_2,gas}/2, \quad (6)$$

where $\mu_{Ti,bulk}$, $\mu_{C,bulk}$, and $\mu_{N_2,gas}$ are the chemical potentials of Ti, C, and N in their stable elemental forms. Bulk Ti and C are assumed to be in the close-packed hexagonal and graphite structures, respectively, and the most stable elemental state of N is assumed to be gas phase N_2. In addition, to avoid segregation of the binary compounds from TiC_xN_{1-x}, the following inequalities must be satisfied:

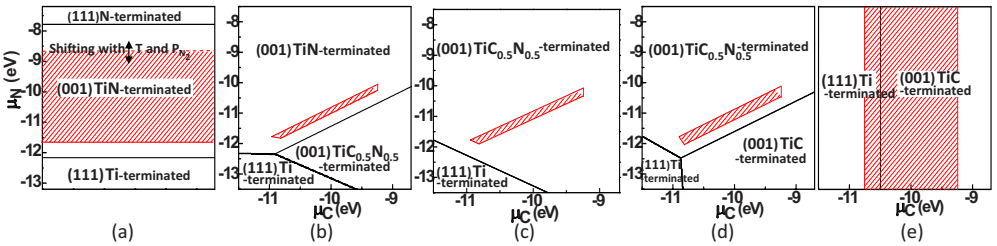

FIG. 3. (Color online) Stability of TiC_xN_{1-x} surfaces for (a) $x=0$, (b) $x=0.25$, (c) $x=0.5$, (d) $x=0.75$, and (e) $x=1.0$. The lowest energy surface for each (μ_C, μ_N) combination is indicated. The boundaries between two different lowest energy surfaces are represented by black lines. The hatched area represents the allowed ranges of μ_C and μ_N within which TiC_xN_{1-x} is stable to decomposition. In (a) and (e), surface energies depend only on μ_N and μ_C, respectively. The upper boundary in (a) can shift based on the T and P_{N_2}.

$$\mu_{Ti} + \mu_C \leq \mu_{TiC,bulk},$$

$$\mu_{Ti} + \mu_N \leq \mu_{TiN,bulk},$$

$$3\mu_C + 4\mu_N \leq \mu_{C_3N_4,bulk}, \tag{7}$$

where $\mu_{TiC,bulk}$, $\mu_{TiN,bulk}$, and $\mu_{C_3N_4,bulk}$ are the chemical potentials of bulk TiC, TiN, and β-C_3N_4, respectively. Equation (4) can be used to eliminate μ_{Ti} from the above inequalities. Neglecting the temperature or T dependence of the chemical potentials of condensed matter allows the replacement of the bulk chemical potentials by the appropriate DFT energies. The T and pressure (P_{N_2}) dependence of $\mu_{N_2,gas}$ may be preserved by expressing the latter as the sum of the DFT energy of N_2, E_{N_2}, and its chemical potential change with T and P_{N_2}, $\Delta\mu_{N_2,gas}(T, P_{N_2})$. With these simplifications, Eqs. (6) and (7) reduce to

$$\mu_C \leq E_{C,bulk},$$

$$\mu_N \leq [E_{N_2} + \Delta\mu_{N_2,gas}(T, P_{N_2})]/2,$$

$$3\mu_C + 4\mu_N \leq E_{C_3N_4,bulk},$$

$$x\mu_C + (1-x)\mu_N \geq E_{TiC_xN_{1-x},bulk} - E_{Ti,bulk},$$

$$\mu_C - \mu_N \leq (E_{TiC_xN_{1-x},bulk} - E_{TiC,bulk})/(x-1),$$

$$\mu_C - \mu_N \geq (E_{TiC_xN_{1-x},bulk} - E_{TiN,bulk})/(x). \tag{8}$$

Using the above inequalities, we demarcate regions of "allowed" chemical potentials by the hatched area in Fig. 3, representing the (μ_C, μ_N) combination for which ternary TiC_xN_{1-x} will be stable to decomposition. We note that, depending on the composition, the hatched area falls either entirely or mostly within (001) regions. In the case of TiN [Fig. 3(a)], owing to the T and P_{N_2} dependence of μ_N, the upper boundary of the allowed region could shift into the (111) N-terminated region. We note that the T and P_{N_2} dependence of $\Delta\mu_{N_2,gas}$ has not been explicitly taken into account as its effect is minor in the case of pure TiN and irrelevant in the case of the other alloys. Also, in the case of TiC [Fig. 3(e)], the (111) surface may be favored for a small range of μ_C. However, these excursions of the hatched area into non-(001) regions are minor. Based on this analysis, we predict that the (001) surfaces of TiC_xN_{1-x} (with surface terminations depending on the bulk composition) are the most stable surfaces among the surfaces considered.

Next, using established techniques,[16,17] we determined the work function for each of the surfaces considered above. In this method, the planar averaged local electronic potential normal to the surface and that of the corresponding bulk along the same direction are matched, yielding the work function as the difference between the vacuum and the Fermi energy. Figure 4(a) shows the work function of the stable surfaces for each of the five TiC_xN_{1-x} compositions considered, along with available prior theoretical[3] (solid circles) and experimental[4,5] (open circles) results. To aid in a systematic evaluation of trends across surface orientations and terminations, the work function results for all surfaces considered are collected and portrayed in Fig. 4(b). Several

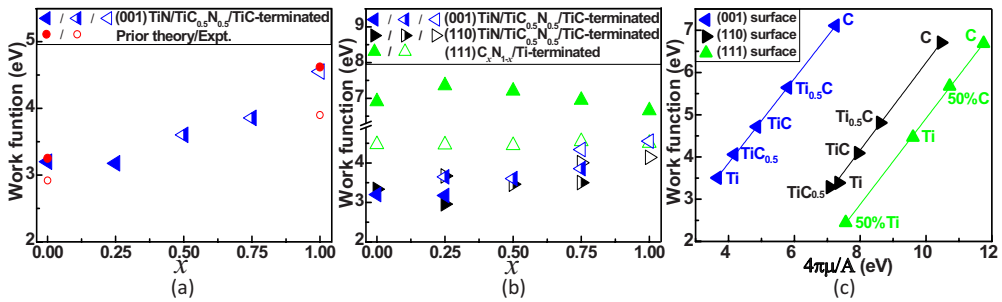

FIG. 4. (Color online) (a) Work function of the stable surfaces of TiC_xN_{1-x} alloys versus composition. (b) Work function results for all TiC_xN_{1-x} surface orientations and terminations considered. (c) Work function versus $4\pi\mu/A$ for TiC surfaces, where μ and A are the surface dipole moment and the surface area. The surface composition is shown beside each data point.

interesting observations can be made. (1) Among the stable surfaces [cf. Fig. 4(a)], we see that the work function increases monotonically from the pure TiN value of 3.2 eV to the pure TiC value of 4.6 eV. (2) Our estimates for the (001) surfaces of the pure binaries are in excellent agreement with prior DFT determinations.[3] (3) However, these determinations for the (001) surfaces deviate from the corresponding experimental values by ~0.3 eV for TiN (Ref. 4) and by ~0.6 eV for TiC (Ref. 5); this discrepancy is presumably because the systems considered experimentally were off stoichiometric ($TiC_{0.94}$),[5] containing a significant density of point defects. (4) For each alloy composition, the work function depends significantly on the surface orientation and termination [cf. Fig. 4(b)], varying by as much as 2.5–4.4 eV depending on the composition. Particularly noteworthy are the C_xN_{1-x}-terminated (111) surfaces which display the highest work function.

In order to further clarify the last two of the above mentioned observations, we have performed a limited number of computations involving defective (001), (110), and (111) TiC surfaces. Defect-free (001) and (110) TiC surfaces are stoichiometric and contain two Ti and two C atoms. By successively removing C or Ti atoms from the surface layer, the surface composition can be varied from 0% C to 0% Ti. The (111) TiC surface is nonstoichiometric and can be either Ti or C terminated, with two atoms per layer as studied here. Here again, starting with the C-terminated (Ti-terminated) surface and by successive removal of the surface C (Ti) atoms, one could create a range of surface compositions for the same orientation. For each of these cases, the work function, as well as the surface dipole moment (μ) per unit area (A), was computed. Figure 4(c) shows a plot of the relationship between these two quantities for each of the three surface orientations. As can be seen, the expected linear behavior[17] with a slope of 1 was obtained for each case. Interestingly, decreasing surface C (or increasing surface Ti) content results in a drastic decrease in the surface dipole moment and the work function. These findings explain the apparent discrepancy between our results for stoichiometric slabs and experimental determinations for the (001) surface that may have involved C-deficient situations. We thus conclude that surface terminations have a *much stronger influence* on the work functions than bulk alloy compositions. This conclusion is expected to hold true for ordered TiC_xN_{1-x} systems (considered here) as well as random TiC_xN_{1-x} alloys.

In summary, we have performed DFT studies of ordered TiC_xN_{1-x} alloys in an attempt to identify the critical factors that control work functions. We find that the most stable surfaces across the compositions considered are the (001) type of surfaces. The work function of these stable surfaces increases monotonically from the pure TiN value of 3.2 eV to the pure TiC value of 4.6 eV. However, this variation is far surpassed by the dependence of the work function on the surface termination and stoichiometry (regardless of the alloy composition). For instance, the work function systematically increases with decreasing Ti content at the surface. Work function "tuning" may thus be accomplished by suitably controlling the surface chemistry for any TiC_xN_{1-x} alloy composition.

Financial support of this work through a grant from the National Science Foundation (NSF) and computational support through a NSF Teragrid Resource Allocation are gratefully acknowledged.

*rampi@ims.uconn.edu

[1] J. Robertson, Rep. Prog. Phys. **69**, 327 (2006).
[2] S.-H. Joo, C.-R. Paik, and K.-H. Lee, U.S. Patent No. 5,795,817 (18 August 1998); J. K. Schaeffer, C. Capasso, R. Gregory, D. Gilmer, L. R. C. Fonseca, M. Raymond, C. Happ, M. Kottke, S. B. Samavedam, P. J. Tobin, and B. E. White, J. Appl. Phys. **101**, 014503 (2007).
[3] K. Kobayashi, Surf. Sci. **493**, 665 (2001); E. Wimmer, A. Neckel, and A. J. Freeman, Phys. Rev. B **31**, 2370 (1985).
[4] Y. Saito, S. Kawata, H. Nakane, and H. Adachi, Appl. Surf. Sci. **146**, 177 (1999).
[5] C. Oshima, T. Tanaka, M. Aono, R. Nishitani, S. Zaima, and F. Yajima, Appl. Phys. Lett. **35**, 822 (1979).
[6] G. Kresse and J. Furthmuller, Phys. Rev. B **54**, 11169 (1996).
[7] J. P. Perdew, J. A. Chevary, S. H. Vosko, K. A. Jackson, M. R. Pederson, D. J. Singh, and C. Fiolhais, Phys. Rev. B **46**, 6671 (1992).
[8] M. Marlo and V. Milman, Phys. Rev. B **62**, 2899 (2000).
[9] L. E. Toth, *Transition Metal Carbides and Nitrides* (Academic, New York, 1971); T. Fujihana, M. Taniguchi, Y. Okabe, and M. Iwaki, Surf. Coat. Technol. **83**, 120 (1996).
[10] D. L. Price, J. M. Wills, and B. R. Cooper, Phys. Rev. Lett. **77**, 3375 (1996); N. Cruz Hernandez, J. Garciani, and J. F. Sanz, Surf. Sci. **541**, 217 (2003).
[11] W. Lengauer, S. Binder, K. Aigner, P. Ettmayer, A. Guillou, J. Debuigne, and G. Groboth, J. Alloys Compd. **217**, 137 (1995).
[12] I.-J. Jung, S. Kang, S.-H. Jhi, and J. Ihm, Acta Mater. **47**, 3241 (1999).
[13] W. Ensinger and A. Schröer, Surf. Coat. Technol. **103-104**, 168 (1998).
[14] H. O. Pierson, *Handbook of Refractory Carbides and Nitrides: Properties, Characteristics and Applications* (Noyes, Westwood, NJ, 1996); A. Azushima, Y. Tanno, H. Iwata, and K. Aoki, Wear **265**, 1017 (2008).
[15] K. Reuter and M. Scheffler, Phys. Rev. B **65**, 035406 (2001); S. J. Jenkins, *ibid.* **70**, 245401 (2004).
[16] C. G. Van de Walle and R. M. Martin, Phys. Rev. B **34**, 5621 (1986).
[17] R. Ramprasad, P. von Allmen, and L. R. C. Fonseca, Phys. Rev. B **60**, 6023 (1999).